

A Comprehensive Evaluation and Benchmark for Person Re-Identification: Features, Metrics, and Datasets

Srikrishna Karanam^{*a}, Mengran Gou^{*b}, Ziyang Wu^a, Angels Rates-Borras^b,
Octavia Camps^b, Richard J. Radke^a

^aDepartment of Electrical, Computer, and Systems Engineering, Rensselaer
Polytechnic Institute

^bDepartment of Electrical and Computer Engineering, Northeastern University

Abstract. Person re-identification (re-id) is a critical problem in video analytics applications such as security and surveillance. The public release of several datasets and code for vision algorithms has facilitated rapid progress in this area over the last few years. However, directly comparing re-id algorithms reported in the literature has become difficult since a wide variety of features, experimental protocols, and evaluation metrics are employed. In order to address this need, we present an extensive review and performance evaluation of single- and multi-shot re-id algorithms. The experimental protocol incorporates the most recent advances in both feature extraction and metric learning. To ensure a fair comparison, all of the approaches were implemented using a unified code library that includes 6 feature extraction algorithms and 21 metric learning and ranking techniques. All approaches were evaluated using a new large-scale dataset that closely mimics a real-world problem setting, in addition to 13 other publicly available datasets: VIPeR, GRID, CAVIAR, 3DPeS, PRID, V47, WARD, SAIVT-SoftBio, CUHK03, RAiD, iLIDSVID, HDA+ and Market1501. The evaluation codebase and results will be made publicly available for community use.

1 Introduction

Person re-identification, or re-id, is a critical task in most surveillance and security applications [1, 2] and has increasingly attracted attention from the computer vision community [3–21]. The fundamental re-id problem is to compare a person of interest as seen in a “probe” camera view to a “gallery” of candidates captured from a camera that does not overlap with the probe one. If a true match to the probe exists in the gallery, it should have a high matching score, or rank, compared to incorrect candidates.

Since the body of research in re-id is now quite large, we can begin to draw conclusions about the best features and metric learning algorithms for re-id. In this paper, we present a careful, fair, and comprehensive evaluation of re-id

^{*}These two authors contributed equally to this work.

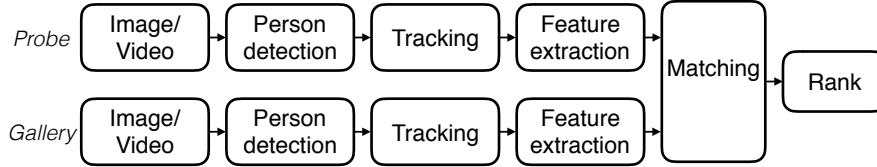


Fig. 1. A typical end-to-end re-id system pipeline.

algorithms on a wide variety of benchmark datasets. In particular, we evaluate 160 different combinations of feature extraction and metric learning algorithms on 7 single-shot re-id datasets and 460 different algorithm combinations on 7 multi-shot re-id datasets, making the proposed study the **largest and most comprehensive** re-id benchmark to date. As part of the evaluation, we built a **public code library** with an easy-to-use input/output code structure and uniform algorithm parameters that includes 6 contemporary feature extraction and 21 metric learning and ranking algorithms. Both the code library and the complete benchmark results will be made publicly available for community use.

Existing re-id algorithms are typically evaluated on academic re-id datasets [3, 22–28] that are specifically hand-curated to only have sets of bounding boxes for the probes and the corresponding matching candidates. On the other hand, real-world end-to-end surveillance systems include automatic detection and tracking modules, depicted in Figure 1, that generate candidates on-the-fly, resulting in gallery sets that are dynamic in nature. Furthermore, errors in these modules may result in bounding boxes that may not accurately represent a human. While these issues are critical in practical re-id applications, they are not well-represented in the currently available datasets. To this end, our evaluation also includes a **new, large-scale dataset** constructed from images captured in a challenging surveillance camera network from an airport. All the images in this dataset were generated by running a prototype end-to-end real-time re-id system using automatic person detection and tracking algorithms instead of hand-curated bounding boxes.

2 Evaluated Techniques

In this section, we summarize the feature extraction, metric learning, and multi-shot ranking techniques that are evaluated as part of the proposed re-id benchmark, which include algorithms published through CVPR 2015. We anticipate that the benchmark will be updated (along the lines of the Middlebury benchmarks [29, 30]) as new techniques are implemented into our evaluation framework.

2.1 Feature extraction

We consider 6 feature extraction schemes that are commonly used in the re-id literature, summarized in Table 1 (a). In ELF [3], color histograms in the RGB, YCbCr, and HS color spaces, and texture histograms of responses of rotationally invariant Schmid [31] and Gabor [32] filters are computed. In LDFV [33],

local pixel descriptors comprising pixel spatial location, intensity, and gradient information are encoded into the Fisher vector [34] representation. In **gBiCov** [35], multi-scale biologically-inspired features [36] are encoded using covariance descriptors [37]. In **DenseColorSIFT** [8], each image is densely divided into patches, and color histograms and SIFT features are extracted from each patch. In **HistLBP** [12], color histograms in the RGB, YCbCr, and HS color spaces and texture histograms from local binary patterns (LBP) [38] features are computed. In **LOMO** [17], HSV color histograms and scale-invariant LBP [39] features are extracted from the image processed by a multi-scale Retinex algorithm [40], and maximally-pooled along the same horizontal strip.

Feature	Year	Metric	Year	Metric	Year
ELF [3]	ECCV 08	l_2		PCCA [7]	CVPR 12
LDFV [33]	ECCVW 12	FDA [41]	AE 1936	kPCCA [7]	CVPR 12
gBiCov [35]	BMVC 12	ITML [42]	ICML 07	LFDA [10]	CVPR 13
DenseColorSIFT [8]	CVPR 13	MFA [43]	PAMI 07	SVMML[44]	CVPR 13
HistLBP [12]	ECCV 14	LMNN [45]	JMLR 08	kMFA [12]	ECCV 14
LOMO [17]	CVPR 15	RankSVM [4]	BMVC 10	rPCCA [12]	ECCV 14
		PRDC [5]	CVPR 11	kLFDA [12]	ECCV 14
		KISSME [6]	CVPR 12	XQDA [17]	CVPR 15

(a)
(b)

Table 1. Evaluated feature extraction and metric learning methods.

2.2 Metric learning

While using any of the features described in the previous section in combination with the Euclidean distance (l_2) can be used to rank gallery candidates, this would be an unsupervised and suboptimal approach. Incorporating supervision using training data leads to superior performance, which is the goal of metric learning, i.e., learning a new feature space such that feature vectors of the same person are close whereas those of different people are relatively far. We consider 16 metric learning methods that are typically used by the re-id community, summarized in Table 1 (b). Fisher discriminant analysis (FDA) [41], local Fisher discriminant analysis (LFDA) [10], marginal Fisher analysis (MFA) [43], and cross-view quadratic discriminant analysis (XQDA) [17] all formulate a Fisher-type optimization problem that seeks to minimize the within-class data scatter while maximizing between-class data scatter. In practice, scatter matrices are regularized by a small fraction of their trace to deal with matrix singularities. Information-theoretic metric learning (ITML) [42], large-margin nearest neighbor (LMNN) [45], relative distance comparison (PRDC) [5], keep-it-simple-and-straightforward metric (KISSME) [6], and pairwise constrained component analysis (PCCA) [7] all learn Mahalanobis-type distance functions using variants of the basic pairwise constraints principle. kPCCA [7], kLFDA [12], and kMFA [12] kernelize PCCA, LFDA, and MFA, respectively. For these kernel-based methods, we consider the standard **linear**, **exponential (exp)**, **chi2** (χ^2), and **chi2-rbf** (R_{χ^2}) kernels. In **RankSVM** [4], a weight vector that weights the different features

appropriately is learned using a soft-margin SVM formulation. In SVMML [44], locally adaptive decision functions are learned in a large-margin SVM framework.

2.3 Multi-shot ranking

While most re-id algorithms are single-shot, i.e. features are extracted from a single probe image of the person of interest, the multi-shot scenario, in which features are extracted from a series of images of the person of interest, is arguably more relevant to video analysis problems. The simplest way to handle multi-shot data is to compute the average feature vector for each person, effectively resulting in a single-shot problem. However, we also evaluated several algorithms that inherently address multi-shot data, treating it as an image set and constructing affine hulls to compute the distance between a gallery and a probe person. Specifically, we considered the AHISD [46], SANP [47], and RNP [48] algorithms. While these methods were proposed in the context of face recognition, the basic notion of image set matching applies to re-id as well. We also evaluated multi-shot methods based on sparse ranking, in which re-id is posed as a sparse recovery problem. Specifically, we considered SRID [49] and ISR [50].

2.4 Techniques not (yet) considered

In this section, we briefly describe methods that do not fall into the three general categories discussed above. These methods are currently not a part of the proposed benchmark, but will be evaluated in a future release.

Following the recent advances achieved by deep convolutional neural networks (CNN) [51], there has been considerable interest in CNNs in the context of re-id [52–54]. While we anticipate that some of these CNN-based methods may give superior performance than the best performing method in our benchmark, they are currently not a part of the benchmark due to the non-availability of source code. Post-rank learning methods, involving verifying the validity of the generated results, have also been applied to the re-id problem [55, 56]. Other techniques employed in re-id which are not evaluated in this study include unsupervised learning [8, 22, 57], attribute learning [58–60], ensemble methods [61–63] and mid-level representation learning [13]. A more comprehensive survey of these and other related methods can be found in the book by Gong *et al.* [2] and papers by Satta [64], Vezzani [65], and Bedagkar-Gala and Shah [66].

3 Datasets

In this section, we briefly summarize the various publicly available datasets that are used as part of this benchmark evaluation. Table 2 provides a statistical summary of each dataset. Based on difficult examples¹, we also annotate each dataset with challenging attributes from the following: viewpoint variations (VV), illumination variations (IV), detection errors (DE), occlusions (OCC), background

¹ Provided as part of the supplementary material.

clutter (BC), and low-resolution images (LR). We also indicate the number of bounding boxes (BBox) and cameras (cam) in each dataset, and the means by which the bounding boxes were obtained: using hand-labeling (hand), aggregated channel features [67] (ACF), or the deformable parts model detector [68] (DPM).

Dataset	# people	# BBox	# distractors	# cam	label	Attributes
VIPeR	632	1,264	0	2	hand	VV,IV
GRID	250	500	775	2	hand	VV,BC,OCC,LR
CAVIAR	72	1,220	0	2	hand	VV,LR
3DPeS	192	1,011	0	8	hand	VV,IV
PRID	178	24,541	0	2	hand	VV,IV
V47	47	752	0	2	hand	-
WARD	70	4,786	0	3	hand	IV
SAIVT-Softbio	152	64,472	0	8	hand	VV,IV,BC
CUHK03	1,360	13,164	0	2	DPM/hand	VV,DE,OCC
RAiD	43	6,920	0	4	hand	IV
iLIDSVID	300	42,495	0	2	hand	VV,IV,BC,OCC
HDA+	74	2,976	0	12	ACF/hand	VV,IV,DE
Market1501	1,501	32,643	2,793+500K	6	DPM	VV,DE,LR
Airport	1,382	8,664	31,238	6	ACF	VV,IV,DE,BC

Table 2. The characteristics of the 14 datasets of the re-id benchmark.

VIPeR [3] consists of 632 people from two disjoint views. Each person has only one image per view. GRID [69] has 250 image pairs collected from 8 non-overlapping cameras. To mimic a realistic scenario, 775 non-paired people are included in the gallery set, which makes this dataset extremely challenging. CAVIAR [22] is constructed from two cameras in a shopping mall. Of the 72 people, we only use 50 people who have images from both cameras. In the case of 3DPeS [24], the re-id community uses a set of selected snapshots instead of the original video, which includes 192 people and 1,011 images. PRID [23] is constructed from two outdoor cameras, with 385 tracking sequences from one camera and 749 tracking sequences from the other camera. Among them, only 200 people appear in both views. To be consistent with previous work [26], we use the same subset of the data with 178 people. V47 [70] contains 47 people walking through two indoor cameras. WARD [25] collects 4,786 images of 70 people in 3 disjoint cameras. SAIVT-Softbio [71] consists of 152 people as seen from a surveillance camera network with 8 cameras. To be consistent with existing work [71], we use only two camera pairs: camera 3 and camera 8 (which we name SAIVT-38) and camera 5 and camera 8 (which we name SAIVT-58). CUHK03 [52] has 1360 people and 13,164 images from 5 disjoint camera pairs. Both manually labeled bounding boxes and automatically detected bounding boxes using the DPM detector [68] are provided. We only use the detected bounding boxes in our experiments. RAiD [27] includes 43 people as seen from two indoor and two outdoor cameras. iLIDSVID [26] includes 600 tracking sequences for 300 people from 2 non-overlapping cameras in an airport. HDA+ [72] was proposed to be a testbed for an automatic re-id system. Fully labeled frames for 30-minute long

videos from 13 disjoint cameras are provided. Since we only focus on the re-id problem, we use pre-detected bounding boxes generated using the ACF [67] detector. **Market1501** [73] has 1,501 people with 32,643 images and 2,793 false alarms from a person detector [68]. Besides these, an additional 500,000 false alarms and non-paired people are also provided to emphasize practical problems in re-id. **Airport** is the new dataset we introduce in the next section.

3.1 A new, real-world, large-scale dataset

In this section, we provide details about a new re-id dataset we designed for this benchmark. The dataset was created using videos from six cameras of an indoor surveillance network in a mid-sized airport. The cameras cover various parts of a central security checkpoint area and three concourses. Each camera has 768×432 pixels and captures video at 30 frames per second. 12-hour long videos from 8 AM to 8 PM were collected from each of these cameras. Under the assumption that each target person takes a limited amount of time to travel through the network, each of these long videos was randomly split into 40 five minute long video clips. Each video clip was then run through a prototype end-to-end re-id system comprised of automatic person detection and tracking algorithms. Specifically, we employed the ACF framework of Dollar *et al.* [67] to detect people and a combination of FAST corner features [74] and the KLT tracker [75] to track people and associate any broken “tracklets”.

Since all the bounding boxes were generated automatically without any manual annotation, this dataset accurately mimics a real-world re-id problem setting. A typical fully automatic re-id system should be able to automatically detect, track, and match people seen in the gallery camera, and the proposed dataset exactly reflects this setup. In total, from all the short video clips, tracks corresponding to 9,651 unique people² were extracted. The number of bounding box images in the dataset is 39,902, giving an average of 3.13 images per person. 1,382 of the 9,651 people are paired in at least two cameras. A number of unpaired people are also included in the dataset to simulate how a real-world re-id system would work: given a person of interest in the probe camera, a real system would automatically detect and track all the people seen in the gallery camera. Therefore, having a dataset with a large number of unpaired people greatly facilitates algorithmic re-id research by closely simulating a real-world environment. A sample of the images available in the dataset is shown in Figure 2. As can be seen from the figure, these are the kind of images one would expect from a fully automated system with detection and tracking modules working in a real-world surveillance environment.

3.2 Evaluation protocol

Datasets, and training and testing splits. Based on the number of images for each probe person, we categorize the datasets into either the single-shot or

² Due to tracking errors, only the bounding boxes provided by the ACF detector are fed into the following re-id modules.

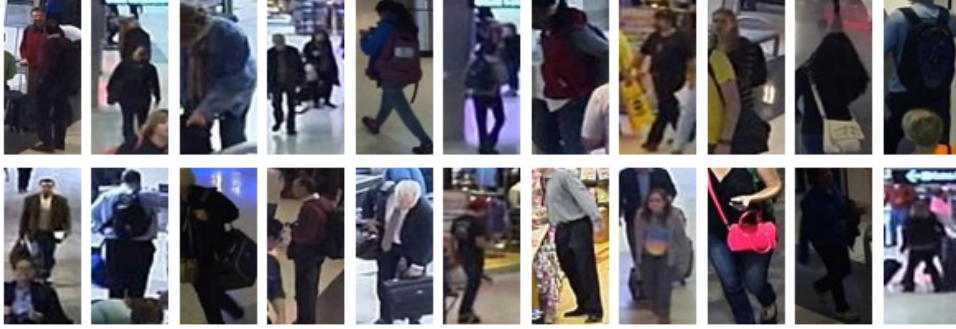


Fig. 2. Samples of images from the proposed **Airport** dataset.

multi-shot setting. We employ the single-shot evaluation protocol for VIPeR, GRID, 3DPeS, CUHK03, HDA+, Market1501 and Airport. For the other 7 datasets, we employ the multi-shot evaluation protocol. In the Airport dataset, we fix one of the 6 cameras as the probe view and randomly pick paired people from 20 of the 40 short clips as the training set, with the rest forming the testing set. In the case of GRID, CUHK03, HDA+ and Market1501, we use the partition files provided by the respective authors. In RAiD, we fix camera 1 as the probe view, resulting in three sub-datasets, RAiD-12, RAiD-13, and RAiD-14, corresponding to the 3 possible gallery views. RAiD-12 has 43 people, of which we use 21 people to construct the training set and the rest to construct the testing set. The other two sub-datasets have 42 people each, which we split into equal-sized training and testing sets. In WARD, we fix camera 1 as the probe view, resulting in two sub-datasets, WARD-12 and WARD-13, corresponding to the 2 possible gallery views. Both these sub-datasets have 70 people each. We split VIPeR, GRID, CAVIAR, 3DPeS, PRID, WARD-12, WARD-13 and iLIDSVID into equal-sized training and testing sets. SAIVT-38 has 99 people, of which we use 31 people for training and the rest for testing. SAIVT-58 has 103 people, of which we use 33 people for training and the rest for testing. Finally, for each dataset, we use 10 different randomly generated training and testing sets and report the overall average results.

Evaluation framework. In the single-shot evaluation scheme, for each dataset, we consider two aspects: type of feature and type of metric learning algorithm. We evaluate all possible combinations of the 6 different features and 16 different metric learning algorithms listed in Table 1. Since we also evaluate four different kernels for the kernelized algorithms, the total number of algorithm combinations is 160.³ In the multi-shot evaluation scheme, we consider three aspects: type of feature, type of metric learning algorithm, and type of ranking algorithm. Additionally, we consider two evaluation sub-schemes: using the average feature vector as the data representative (called **AVER**), and clustering the multiple feature vectors for each person and considering the resulting cluster centers as the representative feature vectors for each person (called **CLUST**). **AVER** effectively converts each dataset into an equivalent single-shot version, giving the same

³ Since LDFV features are not non-negative, we evaluate only **linear** and **exp** kernels in this case.

160 algorithm combinations as above. However, in the case of **CLUST**, we do not consider kernelized metric learning algorithms and other non-typical algorithms such as **RankSVM** and **SVMML** because only **AVER** can be employed to rank gallery candidates. Consequently, we use the remaining 9 metric learning algorithms and the baseline l_2 method, in which we use the features in the original space without any projection. These 10 algorithms are used in combination with the 6 different features and 5 different ranking algorithms, resulting in 300 algorithm combinations for **CLUST**. Therefore, in total, we evaluate 460 different algorithm combinations for each multi-shot dataset.

Implementation and parameter details. We normalize all images of a particular dataset to the same size, which is set to 128×48 for **VIPeR**, **GRID**, **CAVIAR** and **3DPeS** and 128×64 for all other datasets. To compute features, we divide each image into 6 horizontal rectangular strips. A notable exception is **LOMO**, which fixes the patches to be square-shaped, which results in 12 patches for a 128×48 image and 18 patches for a 128×64 image. In metric learning, we set the projected feature space dimension to 40. We set the ratio of the number of negative to positive pairwise constraints to 10.⁴ In the case of **CLUST**, we set the number of clusters to 10, which we determine using the **k-means** algorithm. The entire code library, training and testing splits, and evaluation results will be made available online upon acceptance of the paper.

4 Results and Discussion

We first summarize the results of the overall evaluation, and then discuss several aspects of these results in detail.

The overall cumulative match characteristic (CMC) curves for each of the 18 datasets and sub-datasets are shown in Figure 3. The individual performance of each algorithm combination on all datasets can be found in the supplementary material. As can be seen from the CMC curves, the “spread” in the performance of the algorithms for each dataset is huge, indicating the progress made by the re-id community over the past decade. However, on most datasets, the performance is still far from the point where we would consider re-id to be a solved problem.

In Table 3, we summarize the overall CMC curves by reporting the algorithm combination that achieved the best performance on each dataset as measured by the rank-1 performance. We note that **LOMO** [17] performs the best among the 6 evaluated feature extraction algorithms, with it being a part of the best performing algorithm combination in 5 of the 7 single-shot and nearly all the 11 multi-shot datasets except **V47**. **kLFDA** [12] and **XQDA** [17] are both a part of the best performing algorithm combination in 3 of the 7 single-shot datasets. However, we note that **LOMO-kLFDA_{exp}** gives a mean rank-1 performance of 41.2% across all the single-shot datasets whereas **LOMO-XQDA** gives 38.7%, suggesting that **kLFDA_{exp}** is the best performing metric learning algorithm. Finally, the

⁴ This is set to 1 for **kPCCA** and **rPCCA** on **Market1501** due to system memory issues.

Datasets	Best Combination	1	5	10	15	20
VIPeR	LOMO-XQDA	33.0	62.4	75.3	83.1	87.9
GRID	LOMO-XQDA	17.4	32.4	40.6	46.0	50.0
3DPeS	LOMO-XQDA	44.4	68.8	79.0	84.8	89.0
CUHK03	LOMO-kLFDA _{exp}	55.3	83.3	91.1	93.9	95.6
HDA+	gBiCov-kMFA _{exp}	80.0	88.5	90.0	90.3	90.4
Market1501	HistLBP-kLFDA _{Rχ^2}	46.5	71.1	79.9	84.4	86.9
Airport	LOMO-kLFDA _{exp}	31.9	54.4	68.2	75.6	80.7
PRID	LOMO-KISSME-SRID	83.0	95.3	97.5	99.1	99.3
V47	LDFV-KISSME-AHISD	100.0	100.0	100.0	100.0	100.0
CAVIAR	LOMO-XQDA-AVER	52.0	88.0	96.4	100.0	100.0
WARD-12	LOMO-FDA-RNP	92.3	99.7	100.0	100.0	100.0
WARD-13	LOMO-KISSME-SRID	82.3	98.3	99.1	99.4	100.0
SAIVT-38	LOMO-KISSME-SRID	86.3	98.8	99.6	99.9	99.9
SAIVT-58	LOMO-KISSME-SRID	65.7	86.9	92.4	95.6	96.1
RAiD-12	LOMO-KISSME-SRID	96.4	100.0	100.0	100.0	100.0
RAiD-13	LOMO-FDA-AVER	71.9	95.2	100.0	100.0	100.0
RAiD-14	LOMO-KISSME-SRID	94.8	99.5	100.0	100.0	100.0
iLIDSVID	LOMO-KISSME-SRID	65.5	85.4	91.3	94.1	95.7

Table 3. Top performing algorithmic combinations on each dataset. Read as **feature-metric** for single-shot and **feature-metric-ranking** for multi-shot.

ment are shown in Figure 4(a). As can be noted from these curves, LOMO gives the best results in comparison with other features on VIPeR, GRID, 3DPeS, CUHK03 and Airport. gBiCov and LDFV give the best results on HDA+ and Market1501 respectively. To further study the impact of LOMO, we compare its performance with other feature extraction algorithms without any metric learning. In this experiment, we use the baseline Euclidean distance to rank gallery candidates in the originally computed feature space, which can be regarded as an unsupervised method. As can be noted from the results shown in Figure 4(b), LOMO gives the best performance without any metric learning as well, with the sole exception of HDA+, on which gBiCov gives the best performance. This discussion clearly shows that LOMO is indeed the best performing feature extraction algorithm, suggesting that preprocessing images with a multi-scale Retinex algorithm to achieve illumination invariance and a horizontal local max-pooling operation to achieve pose invariance, as done in LOMO, are critical steps in extracting features for re-id.

Next, we analyze the best performing metric learning algorithm⁶, kLFDA_{exp}. Here, we fix LOMO as the feature extraction algorithm and compare its performance with other metric learning algorithms. As can be seen from the results shown in Figure 4(c), while kLFDA_{exp} gives a significant rank-1 improvement on CUHK03 and Market1501, and comparable performance on VIPeR, 3DPeS and Airport, we do not observe similar trends on other datasets, with different methods giving the best performance. We next analyze the choice of the kernel in kLFDA. In this experiment, we use LOMO with **exp**, **linear**, χ^2 , and R_{χ^2} kernels.

⁶ A discussion on the training time of these algorithms is provided in the supplementary material.

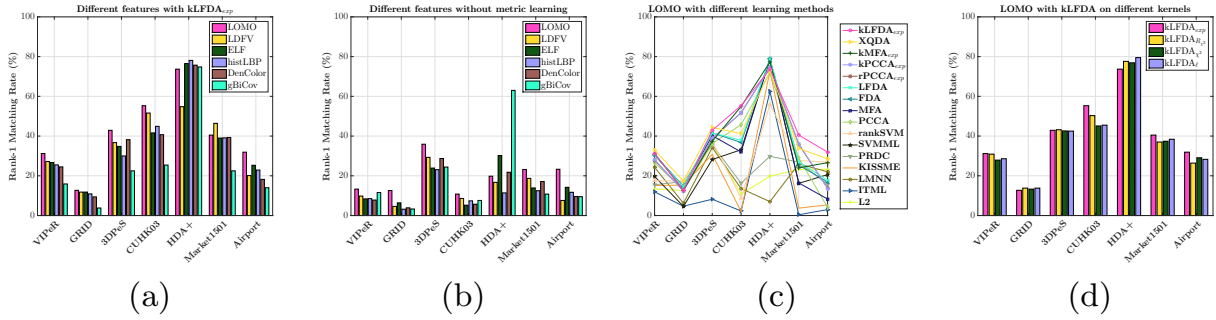


Fig. 4. Rank-1 results for single shot datasets illustrating the impact of LOMO and kLFDA, the best performing feature extraction and metric learning algorithms.

As can be noted from these results shown in Figure 4(d), there is a significant variation in performance with the choice of the kernel, with the rank-1 performance spread being about 4-5% across the four kernels on most datasets. While **exp** gives the best performance on VIPeR, CUHK03, Market1501 and Airport, we do not observe a similar trend on other datasets. However, the rank-1 performance spread shows a similar trend, with a high of about 10% observed on CUHK03.

From the above discussion, we can infer the following: while LOMO clearly emerges as the best performing feature extraction algorithm, the choice of the metric learning algorithm depends on the features chosen. While LOMO-kLFDA_{exp} and LOMO-XQDA both give the best rank-1 performance on the majority of the datasets, LOMO-kLFDA_{exp} gives a higher mean rank-1 performance across all the datasets, illustrating the merits of working in a highly non-linear feature space. Furthermore, the choice of the kernel is dependent on the original feature space, with no clear trends emerging from the results. However, we do note that the **exp** kernel resulted in the best performance on 3 datasets, closely followed by the R_{χ^2} kernel on 2 datasets.

4.2 Multi-shot analysis: features, metric learning, and ranking

Multi-shot re-id involves three aspects: features, metric learning, and ranking. As noted previously, LOMO, KISSME, and SRID emerged as the best performing algorithmic combination. While **AVER** can be considered a naive ranking algorithm in that feature averaging intuitively should result in losing the variation inherent to multi-shot data, it performed surprisingly well, giving the top performance in 2 of the 11 multi-shot datasets (**RAiD-13** and **CAVIAR**). On the other 9 datasets, as expected, a custom ranking algorithm resulted in the best performance, with **SRID** performing the best on 7 of these 9 datasets. In this section, we provide further empirical results analyzing the impact of using a multi-shot ranking algorithm. To this end, we fix LOMO as the feature extraction scheme. To analyze the relative importance of metric learning and multi-shot ranking, we performed several experiments. First, we evaluated the impact of using a multi-shot ranking algorithm instead of **AVER**. Here, we compare the performance of LOMO-AVER and LOMO-SRID without any metric learning. The results are shown

in Figure 5(a). We also compare the performance of LOMO-KISSME-AVER and LOMO-KISSME-SRID. The results are shown in Figure 5(b).

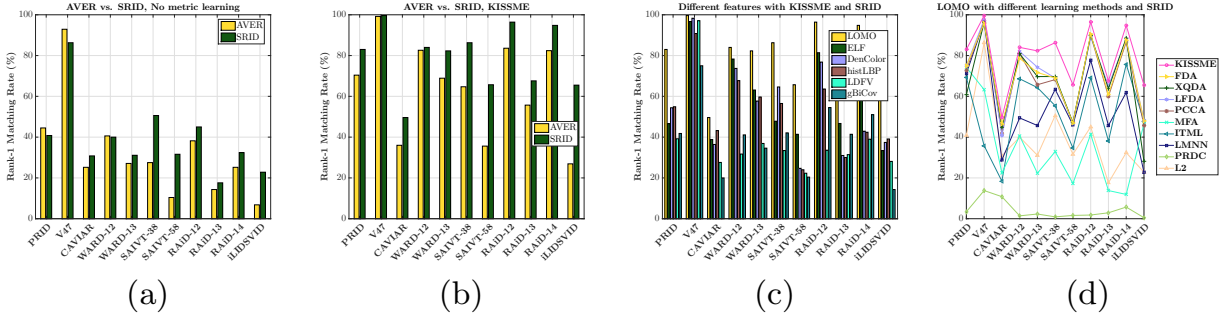


Fig. 5. (a)-(b): Rank-1 performance on multi-shot datasets, illustrating the impact of the best performing multi-shot ranking algorithm, SRID over AVER, naive feature averaging. (c)-(d) Rank-1 performance on multi-shot datasets comparing various feature extraction and metric learning algorithms with SRID as the ranking algorithm.

As can be noted from these two graphs, with a few exceptions (PRID, WARD-12, and V47 without metric learning), SRID generally gives superior performance when compared to AVER regardless of the feature space. These results suggest that using a multi-shot ranking algorithm that exploits the inherent structure of the data instead of naive feature averaging will give better performance. The results also indicate that a multi-shot ranking algorithm in itself is not sufficient to give good performance. Combining a metric learning algorithm with the ranking technique will provide a significant performance boost, as can be noted from Figure 5(b). Next, we analyze the performance of the feature extraction and metric learning algorithms and compare the observed trends with those in the single-shot case. In the feature extraction case, we fix SRID as the ranking algorithm and KISSME as the metric learning algorithm. The rank-1 results for this experiment are shown in Figure 5(c). We see very clear trends in this case, with LOMO consistently giving the best results across all the datasets. These results are not surprising given the strong performance of LOMO in the single-shot case. In the metric learning case, we fix SRID as the ranking algorithm and LOMO as the feature extraction algorithm, with Figure 5(d) showing the rank-1 results. We see very clear trends in this case as well, with KISSME giving the best results across all datasets.

4.3 Additional observations: PCA, features, and attributes

In this section, we report additional empirical observations. Most contemporary feature extraction schemes produce high-dimensional data, introducing significant computational overhead. To this end, we analyze the impact of an unsupervised dimensionality reduction scheme, principal component analysis (PCA). We fix LOMO as the feature extraction scheme and perform experiments with and without PCA. We set the dimension of the PCA-reduced space to 100. The results are shown in the first two bars (pink and yellow) in Figure 6(a) and 6(b). With the exception of Market1501, GRID, HDA+ and 3DPeS, results without PCA are better than those with PCA, suggesting it does not generally help boost

performance. Next, we analyzed the impact of the number-of-strips parameter in the best feature extraction algorithm, LOMO. To this end, we performed experiments with 6, 9, 15, and 24 horizontal strips in LOMO, with Euclidean distance as the metric. The results are shown in Bars 2–5 in Figure 6(a) and 6(b). While it is reasonable to expect superior performance as we increase the number of strips, the results show this is not the case. In fact, we do not observe consistent trends to draw any conclusion. However, we do note that using 6 strips seems to be a reasonable choice. Finally, we analyzed the performance of the different feature extraction schemes with respect to the different attributes used to characterize datasets in Table 2. The goal of this experiment is to study which features are good in certain scenarios. To this end, we use Euclidean distance as the metric, and in the multi-shot case, AVER as the ranking algorithm, and report the mean rank-1 performance on all datasets for each attribute group. The results obtained are shown in Figure 6(c) and 6(d) for the single-shot and multi-shot cases, respectively.

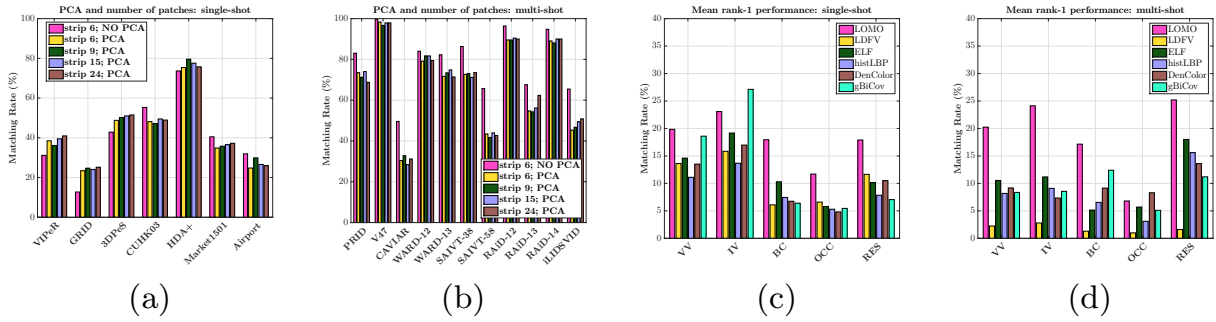


Fig. 6. Rank-1 performance on (a) single-shot and (b) multi-shot datasets illustrating the impact of PCA and number of strips. (c)-(d) Mean rank-1 performance across all single- and multi-shot datasets with respect to various attributes and features.

These results provide further evidence for the effectiveness of LOMO, which resulted in the best mean rank-1 performance across all the attribute groups, except IV in the single-shot case due to the significantly higher rank-1 rate of gBiCov on HDA+. An interesting observation from these results is the strong performance of ELF in spite of being a relatively old feature extraction scheme, giving the next best performance for BC in the single-shot case and VV, IV, and LR in the multi-shot case. Restating the obvious, these results suggest the importance of accurately modeling human appearance in terms of both color and texture features.

4.4 Impact of datasets on re-id research

Datasets play an extremely important role in validating a newly proposed algorithm. From Table 3, we note that the V47 dataset can be considered to be solved, with the best performing algorithm achieving a rank-1 performance of 100%. However, the performance on other multi-shot datasets (RAiD, WARD, SAIVT, iLIDSVID, PRID and CAVIAR) is still far from ideal. These datasets therefore present opportunities and challenges to develop better algorithms. A similar argument holds for the single-shot case. The performance on VIPeR is still very

low despite it being the most popular dataset in the re-id community. The performance on **GRID** is the lowest (17.4% at rank-1) and this is in part due to the presence of a large number of distractor people in the gallery. The newly proposed **Airport** dataset has the next lowest performance (31.9% at rank-1). This is due to the presence of a large distractor set as well as significant real-world challenges described in Section 3.1. As in the multi-shot case, the overall performance on all 7 single-shot datasets can be improved by designing better algorithms, some suggestions for which are discussed in Section 5.

Our categorization of datasets according to their attributes also provides a useful reference point for constructing new datasets. We note that none of the 14 datasets have all 6 attributes. Furthermore, none of these datasets are large enough, in terms of the number of people and positive examples, to apply some of the recent algorithmic advances in feature learning using CNNs [76–78]. We believe focusing on these aspects while collecting new datasets would help accelerate progress in person re-id.

5 Conclusions and future research directions

In this work, we presented a new, large-scale dataset that accurately reflects the real-world person re-identification problem. We conducted large-scale experiments on the new dataset as well as 13 existing datasets, producing a comprehensive re-id evaluation and benchmark that we believe will be extremely valuable to the re-id community.

Based on our results and analysis, we posit important research directions that could be potential candidates for developing better algorithms to improve re-id performance. In feature extraction, a typical approach is to concatenate local features from all image patches or partitions. However, **LOMO**, with its local max-pooling, resulted in the best performance among all the methods. Clearly, such local max-pooling, which is already widely used in convolutional neural networks [51], is important and can be a useful tool in the context of re-id. In the context of multi-shot data, developing feature extraction or learning schemes that specifically exploit the temporal structure of the data [79, 26, 80] will be a natural extension of the existing methods that use only spatial image information. In multi-shot ranking, we demonstrated that using a custom ranking method gives much better performance when compared to using the feature averaging scheme. In practical re-id applications with multi-shot data, an image sequence of a person will typically undergo several variations such as background clutter, occlusion and illumination variations, and developing custom multi-shot ranking algorithms that take all this data variance into account will give better performance. Another promising future research direction in this context would be to integrate multi-shot ranking with metric learning. While most existing methods treat these two topics separately, developing a unified metric learning and multi-shot ranking framework that exploits the several aspects of multi-shot data can potentially lead to further performance gains.

Acknowledgements

This material is based upon work supported by the U.S. Department of Homeland Security under Award Number 2013- ST-061-ED0001. The views and conclusions contained in this document are those of the authors and should not be interpreted as necessarily representing the official policies, either expressed or implied, of the U.S. Department of Homeland Security. Thanks to Michael Young, Jim Spriggs, and Don Kemer for supplying the airport video data.

References

1. Li, Y., Wu, Z., Karanam, S., Radke, R.: Real-world re-identification in an airport camera network. In: Proc. Int. Conf. Distributed Smart Cameras (ICDSC). (2014)
2. Gong, S., Cristani, M., Yan, S., Loy, C.C.: Person re-identification. Volume 1. Springer (2014)
3. Gray, D., Tao, H.: Viewpoint invariant pedestrian recognition with an ensemble of localized features. In: Eur. Conf. Comput. Vision (ECCV). (2008)
4. Prosser, B., Zheng, W.S., Gong, S., Xiang, T.: Person re-identification by support vector ranking. In: Proc. Brit. Mach. Vision Conf. (BMVC). (2010)
5. Zheng, W.S., Gong, S., Xiang, T.: Person re-identification by probabilistic relative distance comparison. In: IEEE Conf. Comput. Vision and Pattern Recognition (CVPR). (2011)
6. Koestinger, M., Hirzer, M., Wohlhart, P., Roth, P.M., Bischof, H.: Large scale metric learning from equivalence constraints. In: IEEE Conf. Comput. Vision and Pattern Recognition (CVPR). (2012)
7. Mignon, A., Jurie, F.: PCCA: A new approach for distance learning from sparse pairwise constraints. In: IEEE Conf. Comput. Vision and Pattern Recognition (CVPR). (2012)
8. Zhao, R., Ouyang, W., Wang, X.: Unsupervised salience learning for person re-identification. In: IEEE Conf. Comput. Vision and Pattern Recognition (CVPR). (2013)
9. Bazzani, L., Cristani, M., Murino, V.: Symmetry-driven accumulation of local features for human characterization and re-identification. *Comput. Vision and Image Understanding (CVIU)* **117**(2) (2013) 130–144
10. Pedagadi, S., Orwell, J., Velastin, S., Boghossian, B.: Local fisher discriminant analysis for pedestrian re-identification. In: IEEE Conf. Comput. Vision and Pattern Recognition (CVPR). (2013)
11. An, L., Kafai, M., Yang, S., Bhanu, B.: Reference-based person re-identification. In: IEEE Int. Conf. Advanced Video and Signal based Surveillance (AVSS), IEEE (2013) 244–249
12. Xiong, F., Gou, M., Camps, O., Sznai, M.: Person re-identification using kernel-based metric learning methods. In: Eur. Conf. Comput. Vision (ECCV). (2014)
13. Zhao, R., Ouyang, W., Wang, X.: Learning mid-level filters for person re-identification. In: IEEE Conf. Comput. Vision and Pattern Recognition (CVPR). (2014)
14. Wu, Z., Li, Y., Radke, R.: Viewpoint invariant human re-identification in camera networks using pose priors and subject-discriminative features. *IEEE Trans. Pattern Anal. Mach. Intell. (T-PAMI)* **37**(5) (2015) 1095–1108

15. Paisitkriangkrai, S., Shen, C., van den Hengel, A.: Learning to rank in person re-identification with metric ensembles. In: IEEE Conf. Comput. Vision and Pattern Recognition (CVPR). (2015)
16. Karanam, S., Li, Y., Radke, R.J.: Person re-identification with discriminatively trained viewpoint invariant dictionaries. In: IEEE Int. Conf. Comput. Vision (ICCV). (2015)
17. Liao, S., Hu, Y., Zhu, X., Li, S.Z.: Person re-identification by local maximal occurrence representation and metric learning. In: IEEE Conf. Comput. Vision and Pattern Recognition (CVPR). (2015)
18. Zheng, W.S., Li, X., Xiang, T., Liao, S., Lai, J., Gong, S.: Partial person re-identification. In: IEEE Int. Conf. Comput. Vision (ICCV). (2015)
19. Li, X., Zheng, W.S., Wang, X., Xiang, T., Gong, S.: Multi-scale learning for low-resolution person re-identification. In: IEEE Int. Conf. Comput. Vision (ICCV). (2015)
20. Messelodi, S., Modena, C.M.: Boosting fisher vector based scoring functions for person re-identification. *Image and Vision Computing (IVC)* **44** (2015) 44–58
21. Chen, D., Yuan, Z., Hua, G., Zheng, N., Wang, J.: Similarity learning on an explicit polynomial kernel feature map for person re-identification. In: IEEE Conf. Comput. Vision and Pattern Recognition (CVPR). (2015) 1565–1573
22. Cheng, D.S., Cristani, M., Stoppa, M., Bazzani, L., Murino, V.: Custom pictorial structures for re-identification. In: Proc. Brit. Mach. Vision Conf. (BMVC). (2011)
23. Hirzer, M., Beleznai, C., Roth, P.M., Bischof, H.: Person re-identification by descriptive and discriminative classification. In: Image Analysis. (2011)
24. Baltieri, D., Vezzani, R., Cucchiara, R.: 3DPeS: 3d people dataset for surveillance and forensics. In: Proceedings of the 2011 joint ACM workshop on Human gesture and behavior understanding. (2011)
25. Martinel, N., Micheloni, C., Piciarelli, C.: Distributed signature fusion for person re-identification. In: Proc. Int. Conf. Distributed Smart Cameras (ICDSC). (2012)
26. Wang, T., Gong, S., Zhu, X., Wang, S.: Person re-identification by video ranking. In: Eur. Conf. Comput. Vision (ECCV). (2014)
27. Das, A., Chakraborty, A., Roy-Chowdhury, A.K.: Consistent re-identification in a camera network. In: Eur. Conf. Comput. Vision (ECCV). (2014)
28. Loy, C.C., Liu, C., Gong, S.: Person re-identification by manifold ranking. In: IEEE Int. Conf. Image Process. (ICIP). (2013)
29. Scharstein, D., Szeliski, R.: A taxonomy and evaluation of dense two-frame stereo correspondence algorithms. *Int. J. Comput. Vision (IJCV)* **47**(1-3) (2002) 7–42
30. Baker, S., Scharstein, D., Lewis, J., Roth, S., Black, M.J., Szeliski, R.: A database and evaluation methodology for optical flow. *Int. J. Comput. Vision (IJCV)* **92**(1) (2011) 1–31
31. Schmid, C.: Constructing models for content-based image retrieval. In: IEEE Conf. Comput. Vision and Pattern Recognition (CVPR). (2001)
32. Fogel, I., Sagi, D.: Gabor filters as texture discriminator. *Biological cybernetics* **61**(2) (1989) 103–113
33. Ma, B., Su, Y., Jurie, F.: Local descriptors encoded by fisher vectors for person re-identification. In: ECCV Workshops. (2012)
34. Sánchez, J., Perronnin, F., Mensink, T., Verbeek, J.: Image classification with the fisher vector: Theory and practice. *Int. J. Comput. Vision (IJCV)* **105**(3) (2013) 222–245
35. Ma, B., Su, Y., Jurie, F.: Covariance descriptor based on bio-inspired features for person re-identification and face verification. *Image and Vision Computing (IVC)* **32**(6) (2014) 379–390

36. Riesenhuber, M., Poggio, T.: Hierarchical models of object recognition in cortex. *Nature neuroscience* **2**(11) (1999) 1019–1025
37. Tuzel, O., Porikli, F., Meer, P.: Pedestrian detection via classification on riemannian manifolds. *IEEE Trans. Pattern Anal. Mach. Intell. (T-PAMI)* **30**(10) (2008) 1713–1727
38. Ojala, T., Pietikäinen, M., Harwood, D.: A comparative study of texture measures with classification based on featured distributions. *Pattern recognition* **29**(1) (1996) 51–59
39. Liao, S., Zhao, G., Kellokumpu, V., Pietikäinen, M., Li, S.Z.: Modeling pixel process with scale invariant local patterns for background subtraction in complex scenes. In: *IEEE Conf. Comput. Vision and Pattern Recognition (CVPR)*. (2010)
40. Jobson, D.J., Rahman, Z.u., Woodell, G.A.: A multiscale retinex for bridging the gap between color images and the human observation of scenes. *IEEE Trans. Image Process. (T-IP)* **6**(7) (1997) 965–976
41. Fisher, R.A.: The use of multiple measurements in taxonomic problems. *Annals of eugenics (AE)* **7**(2) (1936) 179–188
42. Davis, J.V., Kulis, B., Jain, P., Sra, S., Dhillon, I.S.: Information-theoretic metric learning. In: *Int. Conf. Mach. Learning (ICML)*. (2007)
43. Yan, S., Xu, D., Zhang, B., Zhang, H.J., Yang, Q., Lin, S.: Graph embedding and extensions: a general framework for dimensionality reduction. *IEEE Trans. Pattern Anal. Mach. Intell. (T-PAMI)* **29**(1) (2007) 40–51
44. Li, Z., Chang, S., Liang, F., Huang, T.S., Cao, L., Smith, J.R.: Learning locally-adaptive decision functions for person verification. In: *IEEE Conf. Comput. Vision and Pattern Recognition (CVPR)*. (2013)
45. Weinberger, K.Q., Saul, L.K.: Distance metric learning for large margin nearest neighbor classification. **10** (2009) 207–244
46. Cevikalp, H., Triggs, B.: Face recognition based on image sets. In: *IEEE Conf. Comput. Vision and Pattern Recognition (CVPR)*. (2010)
47. Hu, Y., Mian, A.S., Owens, R.: Sparse approximated nearest points for image set classification. In: *IEEE Conf. Comput. Vision and Pattern Recognition (CVPR)*. (2011)
48. Yang, M., Zhu, P., Van Gool, L., Zhang, L.: Face recognition based on regularized nearest points between image sets. In: *IEEE Int. Conf. Automatic Face and Gesture Recognition (FG)*. (2013)
49. Karanam, S., Li, Y., Radke, R.: Sparse re-id: Block sparsity for person re-identification. In: *CVPR Workshops*. (2015)
50. Lisanti, G., Masi, I., Bagdanov, A.D., Del Bimbo, A.: Person re-identification by iterative re-weighted sparse ranking. *IEEE Trans. Pattern Anal. Mach. Intell. (T-PAMI)* **37**(8) (2015) 1629–1642
51. Krizhevsky, A., Sutskever, I., Hinton, G.E.: Imagenet classification with deep convolutional neural networks. In: *Annu. Conf. Neural Inform. Process. Syst. (NIPS)*. (2012)
52. Li, W., Zhao, R., Xiao, T., Wang, X.: DeepReId: Deep filter pairing neural network for person re-identification. In: *IEEE Conf. Comput. Vision and Pattern Recognition (CVPR)*. (2014)
53. Ahmed, E., Jones, M., Marks, T.K.: An improved deep learning architecture for person re-identification. In: *IEEE Conf. Comput. Vision and Pattern Recognition (CVPR)*. (2015)
54. Hu, J., Lu, J., Tan, Y.P.: Deep transfer metric learning. In: *IEEE Conf. Comput. Vision and Pattern Recognition (CVPR)*. (2015)

55. Liu, C., Loy, C.C., Gong, S., Wang, G.: POP: Person re-identification post-rank optimisation. In: IEEE Int. Conf. Comput. Vision (ICCV). (2013)
56. Garcia, J., Martinel, N., Micheloni, C., Gardel, A.: Person re-identification ranking optimisation by discriminant context information analysis. In: IEEE Int. Conf. Comput. Vision (ICCV). (2015)
57. Bak, S., Corvee, E., Bremond, F., Thonnat, M.: Multiple-shot human re-identification by mean riemannian covariance grid. In: IEEE Int. Conf. Advanced Video and Signal based Surveillance (AVSS). (2011)
58. Su, C., Yang, F., Zhang, S., Tian, Q., Davis, L.S., Gao, W.: Multi-task learning with low rank attribute embedding for person re-identification. In: IEEE Int. Conf. Comput. Vision (ICCV). (2015)
59. Layne, R., Hospedales, T.M., Gong, S.: Person re-identification by attributes. In: Proc. Brit. Mach. Vision Conf. (BMVC). (2012)
60. Shi, Z., Hospedales, T.M., Xiang, T.: Transferring a semantic representation for person re-identification and search. In: IEEE Conf. Comput. Vision and Pattern Recognition (CVPR). (2015)
61. Eisenbach, M., Kolarow, A., Vorndran, A., Niebling, J., Gross, H.M.: Evaluation of multi feature fusion at score-level for appearance-based person re-identification. In: Int. Joint Conf. Neural Networks (IJCNN). (2015)
62. Zheng, L., Wang, S., Tian, L., He, F., Liu, Z., Tian, Q.: Query-adaptive late fusion for image search and person re-identification. In: IEEE Conf. Comput. Vision and Pattern Recognition (CVPR). (2015)
63. Martinel, N., Micheloni, C., Foresti, G.L.: A pool of multiple person re-identification experts. *Pattern Recognition Lett. (PRL)* **71** (2016) 23–30
64. Satta, R.: Appearance descriptors for person re-identification: a comprehensive review. *arXiv preprint arXiv:1307.5748* (2013)
65. Vezzani, R., Baltieri, D., Cucchiara, R.: People reidentification in surveillance and forensics: A survey. *ACM Computing Surveys (CSUR)* **46**(2) (2013) 29
66. Bedagkar-Gala, A., Shah, S.K.: A survey of approaches and trends in person re-identification. *Image and Vision Computing* **32**(4) (2014) 270–286
67. Dollár, P., Appel, R., Belongie, S., Perona, P.: Fast feature pyramids for object detection. *IEEE Trans. Pattern Anal. Mach. Intell. (T-PAMI)* **36**(8) (2014) 1532–1545
68. Felzenszwalb, P.F., Girshick, R.B., McAllester, D., Ramanan, D.: Object detection with discriminatively trained part-based models. *IEEE Trans. Pattern Anal. Mach. Intell. (T-PAMI)* **32**(9) (2010) 1627–1645
69. Loy, C.C., Xiang, T., Gong, S.: Time-delayed correlation analysis for multi-camera activity understanding. *Int. J. Comput. Vision (IJCV)* **90**(1) (2010) 106–129
70. Wang, S., Lewandowski, M., Annesley, J., Orwell, J.: Re-identification of pedestrians with variable occlusion and scale. In: ICCV Workshops. (2011)
71. Bialkowski, A., Denman, S., Sridharan, S., Fookes, C., Lucey, P.: A database for person re-identification in multi-camera surveillance networks. In: Int. Conf. Digital Image Computing Techniques and Applicat. (DICTA). (2012)
72. Figueira, D., Taiana, M., Nambiar, A., Nascimento, J., Bernardino, A.: The HDA+ data set for research on fully automated re-identification systems. In: ECCV Workshops. (2014)
73. Zheng, L., Shen, L., Tian, L., Wang, S., Wang, J., Tian, Q.: Scalable person re-identification: A benchmark. In: IEEE Int. Conf. Comput. Vision (ICCV). (2015)
74. Rosten, E., Porter, R., Drummond, T.: Faster and better: A machine learning approach to corner detection. *IEEE Trans. Pattern Anal. Mach. Intell. (T-PAMI)* **32**(1) (2010) 105–119

75. Lucas, B.D., Kanade, T.: An iterative image registration technique with an application to stereo vision. In: Imaging Understanding Workshop. (1981)
76. Simonyan, K., Zisserman, A.: Very deep convolutional networks for large-scale image recognition. arXiv preprint arXiv:1409.1556 (2014)
77. Szegedy, C., Liu, W., Jia, Y., Sermanet, P., Reed, S., Anguelov, D., Erhan, D., Vanhoucke, V., Rabinovich, A.: Going deeper with convolutions. In: IEEE Conf. Comput. Vision and Pattern Recognition (CVPR). (2015)
78. He, K., Zhang, X., Ren, S., Sun, J.: Deep residual learning for image recognition. arXiv preprint arXiv:1512.03385 (2015)
79. Klaser, A., Marszałek, M., Schmid, C.: A spatio-temporal descriptor based on 3d-gradients. In: Proc. Brit. Mach. Vision Conf. (BMVC). (2008)
80. Liu, K., Ma, B., Zhang, W., Huang, R.: A spatio-temporal appearance representation for video-based pedestrian re-identification. In: IEEE Int. Conf. Comput. Vision (ICCV). (2015)